

Towards fast and accurate temperature mapping with proton resonance frequency-based MR thermometry

Jing Yuan¹, Chang-Sheng Mei², Lawrence P. Panych², Nathan J. McDannold², Bruno Madore²

¹Department of Imaging and Interventional Radiology, The Chinese University of Hong Kong, Shatin, New Territories, Hong Kong;

²Department of Radiology, Brigham and Women's Hospital, Harvard Medical School, Boston, MA, USA

ABSTRACT

The capability to image temperature is a very attractive feature of MRI and has been actively exploited for guiding minimally-invasive thermal therapies. Among many MR-based temperature-sensitive approaches, proton resonance frequency (PRF) thermometry provides the advantage of excellent linearity of signal with temperature over a large temperature range. Furthermore, the PRF shift has been shown to be fairly independent of tissue type and thermal history. For these reasons, PRF method has evolved into the most widely used MR-based thermometry method. In the present paper, the basic principles of PRF-based temperature mapping will be reviewed, along with associated pulse sequence designs. Technical advancements aimed at increasing the imaging speed and/or temperature accuracy of PRF-based thermometry sequences, such as image acceleration, fat suppression, reduced field-of-view imaging, as well as motion tracking and correction, will be discussed. The development of accurate MR thermometry methods applicable to moving organs with non-negligible fat content represents a very challenging goal, but recent developments suggest that this goal may be achieved. If so, MR-guided thermal therapies may be expected to play an increasingly-important therapeutic and palliative role, as a minimally-invasive alternative to surgery.

KEY WORDS

Thermometry; focused ultrasound (FUS) thermal therapy; proton resonance frequency (PRF); temperature mapping; pulse sequence; motion

Quant Imaging Med Surg 2012;2:21-32. DOI: 10.3978/j.issn.2223-4292.2012.01.06

Introduction

Magnetic Resonance Imaging (MRI) has evolved from a purely diagnostic imaging modality to a powerful intervention guidance tool. The capability to image temperature is a very attractive feature of MRI and has been used to guide minimally invasive thermal therapies such as radiofrequency (RF) ablation (1), laser ablation (2) and focused ultrasound (FUS) therapy (3). Many parameters of MRI such as the proton density (4,5), spin-

lattice relaxation time (T_1) (6,7), spin-spin relaxation time (T_2) (8), diffusion coefficient (9,10), magnetization transfer (11,12), and proton resonant frequency (PRF) (13-16), are temperature-dependent and have the potential to be used as temperature indicators.

Among temperature-dependent MR parameters, PRF has been shown to be superior to other parameters for temperature monitoring of thermal therapies for several reasons. PRF shows a simple linear correlation with temperature within a relatively large temperature range from $-15\text{ }^{\circ}\text{C}$ to $100\text{ }^{\circ}\text{C}$ (13), covering the temperature range of interest for both low-temperature hyperthermia and high-temperature thermal ablation. In addition, the temperature coefficient of PRF shift is almost constant (13) and almost independent of tissue types and their thermal history, with the notable exception of adipose tissues.

PRF-based temperature imaging generally can be divided into two techniques including spectroscopic imaging and phase imaging. In the spectroscopic approach, PRF shift with temperature is measured from the MR spectra as the resonant

No potential conflict of interest.

Corresponding to: Jing Yuan, PhD. Department of Imaging and Interventional Radiology, The Chinese University of Hong Kong, Shatin, New Territories, Hong Kong. Tel: 852-2632-1036; Fax: 852-2636-0012. Email: jyuan@cuhk.edu.hk.

Submitted Jan 09, 2012. Accepted for publication Jan 26, 2012.

Available at <http://www.amepc.org/qims>

ISSN: 2223-4292 © AME Publishing Company. All rights reserved.



frequency difference between the water peak and an appropriate internal reference peak that is independent of temperature, e.g., lipids. With the use of such an internal reference, PRF-based spectroscopic temperature imaging is insensitive to field drifts and capable of absolute temperature measurements (17). However, a major problem with PRF-based spectroscopic temperature imaging is that temporal and spatial resolution are generally too low for real time monitoring of thermal therapy applications, although techniques have been proposed to partly alleviate this problem (18-20).

While spectroscopic imaging involves measuring signal at many different time points so that frequency information can be extracted, in contrast, phase-imaging sequences typically sample signal for a single echo time (TE) value. Clearly, sampling a single TE value instead of many different ones can enable a considerable decreasing in data requirements, thus allowing faster imaging with better spatial resolution, which may prove especially useful for the real-time monitoring of thermal therapies in moving organs. Such reduction in the amount of sampled data does, however, make phase imaging more vulnerable to corruption by fat signal and/or by field variations unrelated to temperature. Despite these shortcomings, phase-imaging is by far the most commonly used PRF thermometry approach. For this reason, the present review article will first briefly introduce the principle of PRF-based phase temperature mapping, and then focus on important technical advancements in phase-based temperature mapping, including pulse sequence developments and motion tracking and correction methods.

Principles of PRF-based phase temperature mapping

The resonant frequency of protons in a molecule is dependent on the local magnetic field. Due to the nuclear shielding effect of the electrons in water molecules, the local magnetic field B_l that a hydrogen nucleus (proton) experiences is slightly smaller than the external macroscopic main magnetic field strength B_0 . The magnetic field accounting for this shielding effect can be written as:

$$B_l = (1 - \sigma)B_0 \quad [1]$$

where σ denotes the shielding constant. The proton resonant frequency f can be calculated according to the Larmor equation:

$$f = \gamma B_l = (1 - \sigma)\gamma B_0, \quad [2]$$

Where γ is gyromagnetic ratio of hydrogen and equals to 42.58 MHz per Tesla. When temperature rises, the electron screening of hydrogen nuclei becomes stronger. The change of

the shielding constant with temperature can be described by a simple linear relationship:

$$\Delta\sigma(T) = \alpha T, \quad [3]$$

where α is the temperature coefficient of the shielding constant. The value of α is about equal to -0.01 ppm (parts per million) per degree, i.e. $-0.01 \times 10^{-6}/^\circ\text{C}$, over a relatively wide temperature range from -15°C to 100°C , independent of tissue types (21). Details of the influence of temperature on the shielding effect can be found in the literature (22). Note that the independence of the temperature coefficient on tissue type is only valid for aqueous tissues. In adipose tissues, for example, due to the absence of changes in the hydrogen bonds with temperature, the temperature dependence is dominated by susceptibility effects. Thus, the temperature sensitivity for adipose tissues is usually several orders of magnitude lower than that for water and the PRF shift in fat may not be detectable using normal MR imaging methods (23).

The increase of the shielding effect with temperature leads to a reduced local magnetic field strength and thus a reduced PRF. By using a normal gradient-recalled echo (GRE) imaging pulse sequence, the change in PRF can be detected via a phase change in the heated area, where the amount of the phase change is dependent on the echo time (TE) applied (14). When acquiring dynamic multiple phase images before, during and after heating, the phase differences of these dynamic images are proportional to the temperature dependent PRF change and TE. Temperature changes, $\Delta T(t)$, can be calculated by:

$$\Delta T(t) = \frac{\Delta\Phi(t)}{\gamma \cdot \alpha \cdot B_0 \cdot TE} = \frac{\Phi(t) - \Phi_0}{\gamma \cdot \alpha \cdot B_0 \cdot TE}, \quad [4]$$

where $\Phi(t)$ and Φ_0 are, respectively, the image phase at time t and the phase in a baseline (pre-heating) reference image. If the baseline reference temperature T_0 is known, the absolute temperature $T(t)$ can be calculated as $T(t) = T_0 + \Delta T(t)$.

There are many challenges in achieving the requirements necessary for real-time temperature monitoring of clinical thermal therapies. This is especially true if the goal is not only closed-loop temperature control of thermal therapies in stationary tissues such as brain and uterine fibroids, but also treatments in moving organs such as liver. In order to meet these requirements, an ideal PRF-based phase temperature mapping must provide temperature-dependent images with sufficient spatial resolution along with high phase-difference signal-to-noise ratio (or temperature-to-noise ratio, TNR) covering a reasonably large imaging volume, and acquired at a rapid imaging speed. The high spatial resolution helps to provide good structural images to accurately locate the target lesion and



the surrounding tissues. It also helps to define the edges of the heating focus with phase images of sufficiently high TNR. Spatial coverage of the imaging volume can also be important to detect possible secondary (unintended) heating sites and avoid damage to surrounding healthy tissues. Temporal resolution must be high enough to capture the fast temperature rise and provide nearly real-time temperature feedback and control, in the case of moving organs may need to be sub-second. The temperature accuracy must be sufficient during thermal therapy to avoid the under- or over-heating of target tissues. In addition, the motion-induced lesion displacement for thermal therapies of moving organs has to be compensated and corrected to prevent the possible erroneous heating of healthy tissues.

The following sections of this article will review the challenges in PRF-based phase temperature mapping and discuss technical solutions.

Pulse sequences for PRF-based temperature mapping

As mentioned above, a gradient-recalled echo pulse sequence is the most common pulse sequence type for temperature imaging, due to its simplicity and relatively-high temperature sensitivity. In contrast, the spin echo (SE) pulse sequence and its derivatives such as Fast Spin Echo (FSE), also called Turbo Spin Echo (TSE), or Rapid Acquisition with Refocused Echoes (RARE), are generally not suitable for PRF temperature imaging because the temperature dependent phase dispersion is refocused (24). For GRE pulse sequences, to produce reasonably large phase differences and high TNR for temperature mapping, a relatively long TE may be required. The optimum TE setting in terms of TNR can be calculated as follows. TNR can be defined as

$$TNR = \frac{|\Delta\Phi(\Delta T)|}{\sigma_{\Delta\Phi}}, \quad [5]$$

where $\Delta\Phi(\Delta T)$ and $\sigma_{\Delta\Phi}$ denote the image phase difference and the noise associated with the phase difference at the temperature change of ΔT , respectively. $\sigma_{\Delta\Phi}$ is inversely proportional to the MR signal amplitude, or MR image intensity, thus, TNR becomes proportional to the product of image phase difference $\Delta\Phi(\Delta T)$ and the image intensity S , i.e., $TNR \propto |\Delta\Phi(\Delta T)| \cdot S$. The signal intensity S_{GRE} for a spoiled GRE pulse sequence can be described by the well-known formula as shown in Eq. 6:

$$S_{GRE} = \frac{M_0 \sin \theta (1 - e^{-TR/T_1})}{1 - \cos \theta} e^{-TE/T_2}, \quad [6]$$

where M_0 is the equilibrium longitudinal magnetization and θ is the applied flip angle. TE is the echo time, TR the repetition time, T_1 the longitudinal relaxation time, and T_2^* represents

the loss of transverse signal due to both irreversible decay and reversible loss of coherence. The maximum signal intensity is achieved for a flip angle equal to $\arccos(e^{-TR/T_1})$, which is also called the Ernst angle. By substituting Eq. 6 and the linear correlation between temperature variation and TE into $TNR \propto |\Delta\Phi(\Delta T)| \cdot S$, it can be derived that.

$$TNR \propto TE \cdot e^{-TE/T_2^*}. \quad [7]$$

By differentiating Eq. 7 with respect to TE, it is obtained that the maximum TNR is achieved at an optimal echo time of $TE = T_2^*$ (19,25).

As the T_2^* for tissues can be as long as tens of milliseconds, relatively long TE and TR settings are typically required, which impose limits on acquisition speed. An echo shifting strategy such as principles of echo shifting with train of observations (PRESTO) can be used to achieve TE values that are greater than TR (i.e., $TE > TR$), so that TR can be shortened and acquisition speed increased while keeping TE unchanged (26).

In addition to the normal GRE sequence, fast MRI pulse sequences such as gradient-echo echo-planar imaging (EPI) (27,28) and spiral imaging (29) can also be used for temperature mapping with temperature sensitivity comparable to the GRE sequence, but with higher temporal resolution (up to sub-second level). These pulse sequences employ long readouts covering large portions of k-space (rather than a single line in k-space) to significantly reduce the number of required TRs and thus reduce the acquisition time. In extreme cases, the entire k-space matrix may be covered in a single TR, leading to single-shot imaging. Despite the advantage of high temporal resolution, image-quality problems associated with fast sequences such as EPI must be considered. With EPI for example, spatial resolution, SNR, image distortions, ghosting artifacts and chemical shift artifacts can all prove problematic.

The balanced steady-state free precession (balanced SSFP or b-SSFP) sequence has also been proposed for temperature mapping (30,31). A b-SSFP sequence offers high signal-to-noise ratio efficiency, T_2/T_1 contrast weighting, insensitivity to flow dephasing as well as the extremely short TR values and hence short acquisition times. While signal is refocused at $TE = TR/2$ and no significant temperature-induced phase offsets could be measured at this TE setting, moving the sampling window away from the center of the TR interval allows b-SSFP PRF thermometry to be performed. However, b-SSFP signals can be thought of as a superposition of signals all featuring different temperature sensitivities, and as such the relation between signal phase and temperature in b-SSFP is non-linear (i.e., Eq. 4 does not generally apply). One study attempted to determine the frequency as the slope of a linear fit of the phases



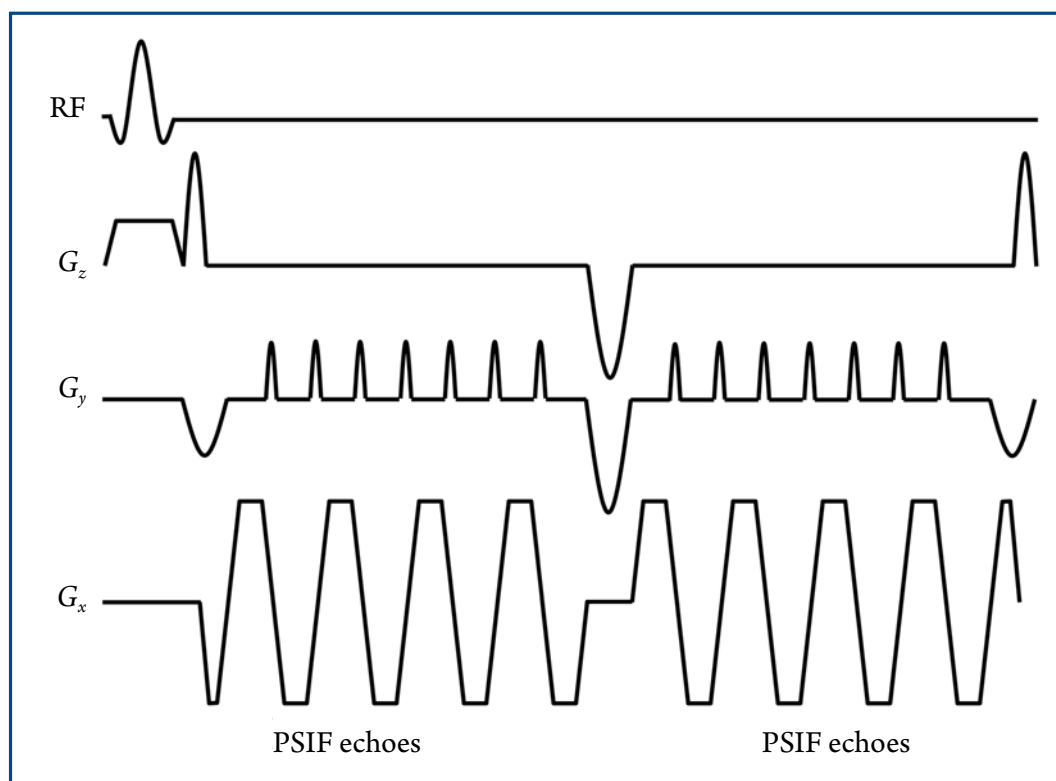


Figure 1. The gradient waveforms of the multipathway pulse sequence for thermal therapy. This sequence features signals from two magnetization pathways: PSIF and FISP echoes, both of which are acquired by EPI readouts. Three blips along the $G_z(t)$ waveform manipulates the magnetization pathways and force PSIF echoes to be acquired first. Acquiring PSIF first and FIPS later allows higher temperature sensitivity for both echoes.

measured at different TEs along the echo train in a multi-echo b-SSFP sequence (30). Another study used a different strategy to obtain the temperature-dependent frequency offset curves from multiple b-SSFP magnitude images using RF pulses applied with different phases. It then correlated the phase shift of curve maxima to the temperature change through circular cross-correlation technique (31). In practice, the non-linearity of phase changes with respect to temperature changes, along with a vulnerability to magnetic field inhomogeneities and associated dark-band artifacts, greatly reduce the appeal of b-SSFP for PRF thermometry.

Recently, Madore *et al.* proposed a novel multipathway sequence for thermal therapy (32). This multipathway sequence can be implemented using single-echo GRE readouts or EPI readouts (Figure 1). Through modifications in the gradient waveforms, this multipathway sequence typically samples two different magnetization pathways, the FISP (fast imaging with steady-state precession) and the inverted FISP (or PSIF). Further (less intense) magnetization pathways could be sampled

as well if so desired. While each pathway has its own temperature sensitivity, signal phase is linearly related to temperature for all of them. Multiple complex images, one from each sampled pathway, are reconstructed and used to obtain temperature maps. Sampling additional pathways has advantages in terms of TNR, and the multiple contrasts available can be used to detect features such as blood vessels (for motion tracking purposes) and tissue damage, at no cost in scan time. While the approach appears to have promise, its applicability for clinical use has yet to be established.

Resolving or suppressing fat signals for accurate thermometry

As mentioned previously, fat has a temperature sensitivity several orders of magnitude lower than water. As a result, it is generally not possible to detect phase changes due to PRF shift in fat. As will be shown, this complicates the use of the PRF method for



temperature mapping when both fat and water are present.

For many tissues containing both fat and water, as may be found in the breast or in a diseased liver tissues, the MR signal \bar{s}_c consists of the complex sum of water (\bar{W}) and fat (\bar{F}) components, each one with its own magnitude and phase as shown in Eq. 8:

$$\bar{s}_c = A_c e^{i\Phi_c} = \bar{W} + \bar{F} = A_w e^{i\Phi_w} + A_f e^{i\Phi_f}, \quad [8]$$

Where A_w , A_f and A_c represent the amplitude of the water, fat, and fat-water combined signals, respectively, while Φ_w , Φ_f and Φ_c represent the corresponding phases. Applying Eq. 4, the measured temperature change (ΔT_m) would be calculated as:

$$\Delta T_m = \frac{\Delta\Phi_c}{\gamma \cdot \alpha \cdot B_0 \cdot TE} = \frac{\Phi_{c1} - \Phi_{c0}}{\gamma \cdot \alpha \cdot B_0 \cdot TE}, \quad [9]$$

where Φ_{c1} and Φ_{c0} are the combined signal phase at the current image and the baseline reference, respectively. Φ_{c0} and Φ_{c1} can be calculated as:

$$\Phi_{c0} = \tan^{-1} \left(\frac{A_w \sin \Phi_{w0} + A_f \sin \Phi_{f0}}{A_w \cos \Phi_{w0} + A_f \cos \Phi_{f0}} \right), \quad [10]$$

$$\Phi_{c1} = \tan^{-1} \left(\frac{A_w \sin(\Phi_{w0} + \Delta T \cdot \gamma \cdot \alpha \cdot B_0 \cdot TE) + A_f \sin \Phi_{f0}}{A_w \cos(\Phi_{w0} + \Delta T \cdot \gamma \cdot \alpha \cdot B_0 \cdot TE) + A_f \cos \Phi_{f0}} \right), \quad [11]$$

with $\Phi_{f0} = \Phi_{w0} + 2\pi \cdot \Delta f \cdot TE$.

In Eq. 11, ΔT is the true temperature change and Δf is the offset frequency of fat at B_0 . Because the phase of the fat signal is nearly temperature-independent, the presence of fat leads to the phase modulation of the combined system and a temperature measurement error (which could be overestimation or underestimation) of $\delta T = \Delta T_m - \Delta T$. Note that this phase modulation by the fat component and the temperature error are dependent on many factors such as B_0 , TE, the amplitude ratio of fat and water, as well as the offset frequency of fat at B_0 (33,34).

Fat suppression, water-selective excitation and fat-water separation are three different strategies that have been employed to address this problem. Fat suppression normally uses spectral selective RF pulses to excite fat and then dephase the excited fat signal using a spoiler gradient. Following the spoiling of the excited fat signal, a normal temperature-sensitive pulse sequence such as GRE is applied to obtain the water-only images for temperature mapping. Disadvantages with this approach are that spectral selective RF pulses have no spatial selectivity and are sensitive to B_1 field inhomogeneities. In addition, the spectral selective RF pulses and the spoiler gradients are also relatively long in duration, and may need to be applied multiple times, all reducing the temporal resolution of temperature mapping. Short tau inversion recovery (STIR) is another option for fat

suppression that utilizes the T_1 difference between fat and water to achieve fat-suppressed magnetization preparation by using an inversion RF pulse and a long inversion time wait prior to the normal image acquisition (35). Problems with STIR are similar to those seen with spectral selective RF pulses such as increased imaging time and sensitivity to B_1 inhomogeneity. An additional problem with employing STIR for temperature mapping is that the acquired image SNR is substantially reduced due to the T_1 relaxation of water, reducing TNR and temperature accuracy.

Water-selective excitation is a more frequently used method for temperature mapping in thermal therapies. Water-selective excitation is usually implemented in the manner of spatial-spectral (SPSP) RF pulses (26,36). SPSP pulses provide both spatial and spectral selectivities, and are compatible with 2D as well as 3D imaging. As opposed to fat suppression techniques such as STIR that employ a fat suppressed magnetization preparation, SPSP pulses are applied in each TR to replace the original excitation RF pulse. SPSP pulses tend to be less sensitive to B_1 inhomogeneities than other fat suppression methods. Although the durations of SPSP pulses may be much longer than a normal excitation pulse, this is often not a severe problem because a long TE is frequently applied anyway in GRE sequences to maximize the TNR.

A significant problem with SPSP pulses is sensitivity to B_0 inhomogeneities. The spectral excitation profile by SPSP pulses is dependent on the pulse duration and the offset frequency between fat and water at a certain magnetic field strength. For high field thermal therapy such as at 3T, with the improved design of SPSP pulses, the duration of SPSP pulses could be greatly reduced to minimize the prolongation of TR for temperature-sensitive sequences, and achieve high temporal resolution temperature mapping (37). It is worth noting that spectral selectivity of fat suppression pulses and SPSP pulses becomes difficult at low field strengths such as 0.5T or lower, due to the small offset frequency of fat relative to water.

Recently, an echo combination method has been proposed to reduce PRF thermometry errors from fat for low-field MR thermometry (38). In this approach, three echoes are acquired and then combined into a single temperature map with predetermined weights to mitigate the temperature overestimation and underestimation at the different TEs, although the remaining error may still not be acceptable for thermal therapies (38). Moreover, the predetermined weighting factors depend on field strength and fat content. Therefore, this echo combination is more of an empirical solution rather than a general one such as that obtained with fat suppression and water-selective excitation.

Fat-water separation methods involve the use of special



reconstruction algorithm to produce individual fat-only and water-only (as well as B_0 map) images from multiple complex images acquired with different TEs. Dixon's method (39,41) and IDEAL (iterative decomposition of water and fat with echo asymmetry and least squares estimation) technique (42) are two representative fat-water separation methods. In a recent study, IDEAL has been proposed for PRF-based temperature mapping, called fat and water thermal MRI (WAF-T-MRI) (43), and temperature maps have been demonstrated on heated phantoms with different ratios of fat and water through off-line reconstruction. A significant advantage of WAF-T-MRI is that it has an inherent independence from artifacts due to B_0 drift during heating. The apparent phase change of the temperature-independent fat signal can be self-referenced to account for the B_0 drift by heating. However, there are still some problems associated with WAF-T-MRI. First, WAF-T-MRI may fail for voxels containing only water or fat. Also, the acquisitions with three or more TEs greatly prolong the scan time and reduce the temporal resolution of temperature imaging. Although the use of multiple echoes in a single TR may alleviate this problem, it, on the other hand, introduces the T_2^* decay along TEs and complicates the reconstruction algorithm. As WAF-T-MRI reconstruction involves intensive computation load, its feasibility for on-line real time temperature mapping and control needs to be further verified in future studies.

Reduced-FOV imaging for increased acquisition speed

For many thermal therapies such as FUS treatment, RF ablation and laser ablation, the intensely-heated regions and the surrounding tissues are contained within a relatively small portion of the FOV. For this reason, reduced field-of-view (rFOV) imaging may prove an especially effective way of speeding up the data acquisition process in MR thermometry. For example, improvements in temporal resolution can help capture fast temperature rises and/or resolve tissue movement. The rFOV imaging using two-dimensional spatially-selective RF (2DRF) pulses has been demonstrated as an effective and efficient method for fast temperature mapping (34,44,45). 2DRF pulses enable spatial selectivity along not only the usual slice selection direction, but also along the phase-encoding direction, as RF energy is deposited in the imaged object while applying time-varying magnetic field gradients along both directions. Only a small region along the phase-encoding direction is excited by the 2DRF pulse, to cover only the heating spots and some surrounding tissues. The size of the phase-encoded FOV

can then be reduced without generating aliasing artifacts. In other words, spatial coverage along the phase-encoding direction is traded for a reduction in the number of phase-encoding steps required and hence scan time. The achievable reduction factor of the phase FOV (and scan time) is dependent on the number of sub-pulses and the total duration of the 2DRF pulses.

As with SPSP pulses, the increased duration of 2DRF pulses compared to the standard slice-select pulse may not be a major issue because one already tends to employ a long TE for temperature mapping. However, 2DRF pulses are also sensitive to B_0 inhomogeneities, susceptibility and the frequency drift during heating, all of which may distort the rFOV excitation profile and compromise the rFOV performance. Furthermore, the reduction of phase FOV also decreases SNR, and thus may reduce TNR and the temperature accuracy. Another problem associated with 2DRF pulses is that insufficiently suppressed signal can be aliased into the reduced FOV if the reduction factor is set too large. The 2DRF pulse must be carefully designed to avoid such aliasing artifact.

A solution that has been proposed to remove or reduce potential aliasing artifacts is the combined use of Fourier encoding of the overlaps using the temporal dimension (UNFOLD) (46) along with the 2DRF pulse. A hybrid use of 2DRF, UNFOLD and parallel imaging (Figure 2) has also been demonstrated to achieve a temporal resolution improvement up to 24-fold compared to the normal GRE sequence (45). The use of 2DRF pulses for temperature mapping has also been demonstrated using a method referred to as MURPS (Multiple Resolutions along Phase-Encode and Slice-Select Directions) (47). In this approach extended volume coverage in the slice direction was obtained without increasing overall scan time (48). It is also worth noting that a careful design of the 2DRF pulses (involving a relatively long pulse duration) can enable their use for both fat suppression and reduced FOV imaging (Figure 3). Such an approach is promising for temperature mapping in moving organs where there is significant adipose tissue (34).

In an extreme case of rFOV imaging, the imaged FOV can be reduced to a 1D line. The line scan technique can be used for this purpose whereby one employs an orthogonal pair of 90° and 180° pulses to excite a 1D column of tissue. A very high temperature sampling rate was demonstrated in gel phantoms employing a line scan echo-planar spectroscopic imaging sequence (LSEPSI) (Figure 4) (49).

Dealing with motion

Although successful clinical applications of MR thermometry have been achieved for many thermal therapies on stationary



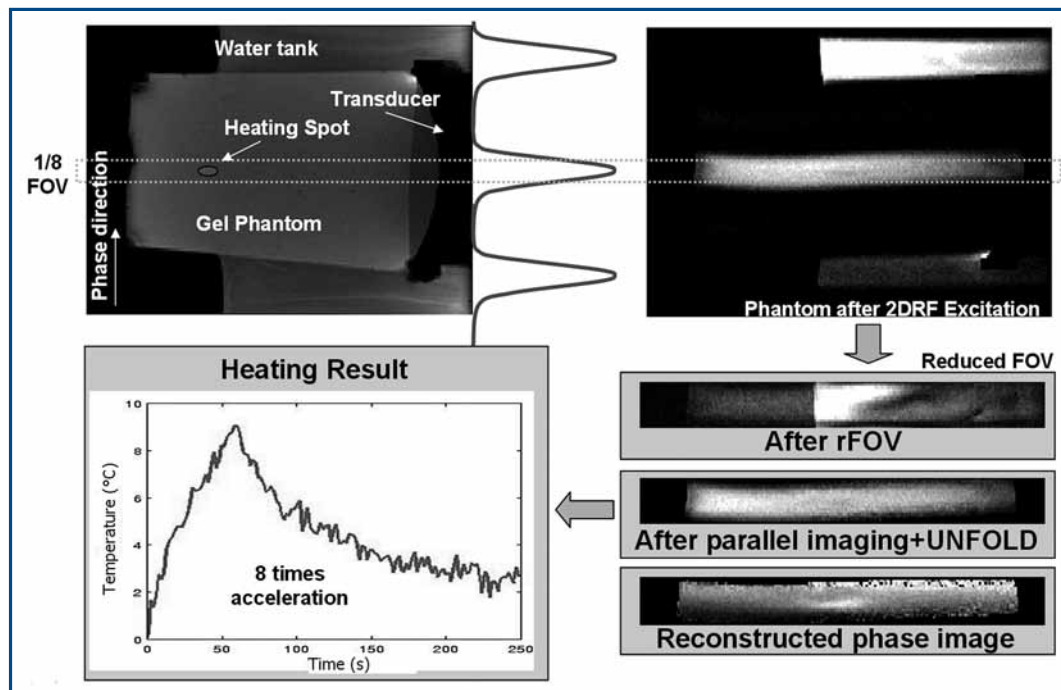


Figure 2. Schematic flow chart illustrates how 2DRF, UNFOLD, and parallel imaging are combined for temperature measurements. *Top-left:* A MR image shows the experimental setup. A water gel phantom and a transducer are immersed in a water tank. The focused ultrasound beam is delivered through the water and focused within the phantom. *Top-right:* 2DRF pulse excites one central lobe and two side lobes. *Bottom-right:* With FOV reduced to one-eighth of its original size, side lobes and vanishing tail of the central lobe are aliased onto the acquired images. However, the wraparounds can be removed by UNFOLD and parallel imaging, leaving only the central lobe. *Bottom-left:* Looking at how the phase changes over time, the temperature estimations are obtained.

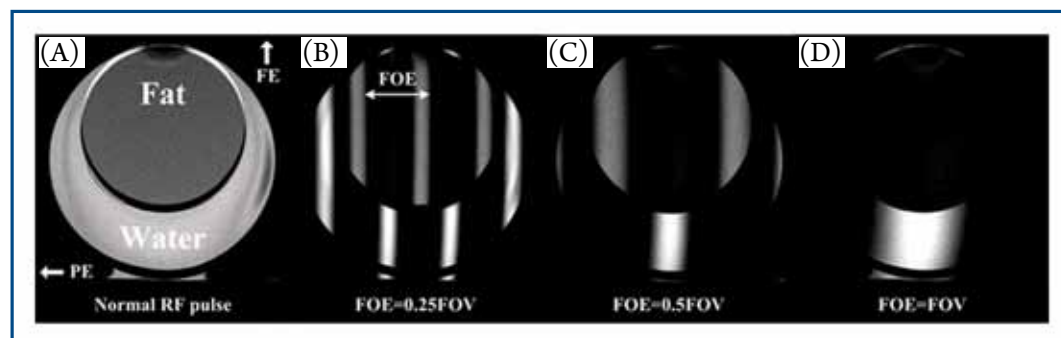


Figure 3. Simultaneous fat suppression and rFOV imaging on a fat-water phantom by using the 2DRF pulse at 3T. A: The reference image produced by the normal FGRE sequence with the normal slice-selective RF pulse. Chemical shift appears along the frequency encoding (FE) direction (vertical) with a narrow receiver bandwidth of 8.06KHz; B-D: Excitation profiles with different field-of-excitation (FOE) values by using a 11-subpulse echo planar 2DRF pulse (each subpulse with 1140 μ s duration). When FOE equals to FOV (D), only a fraction of water at the FOV center is excited.

tissues such as uterine fibroids, real-time temperature monitoring in moving organs, such as liver and kidney, remains a challenge. In this case, MR imaging must fulfill the joint tasks of

temperature monitoring and motion tracking. Many dedicated techniques have been proposed for temperature mapping of moving organs in addition to common motion tracking or



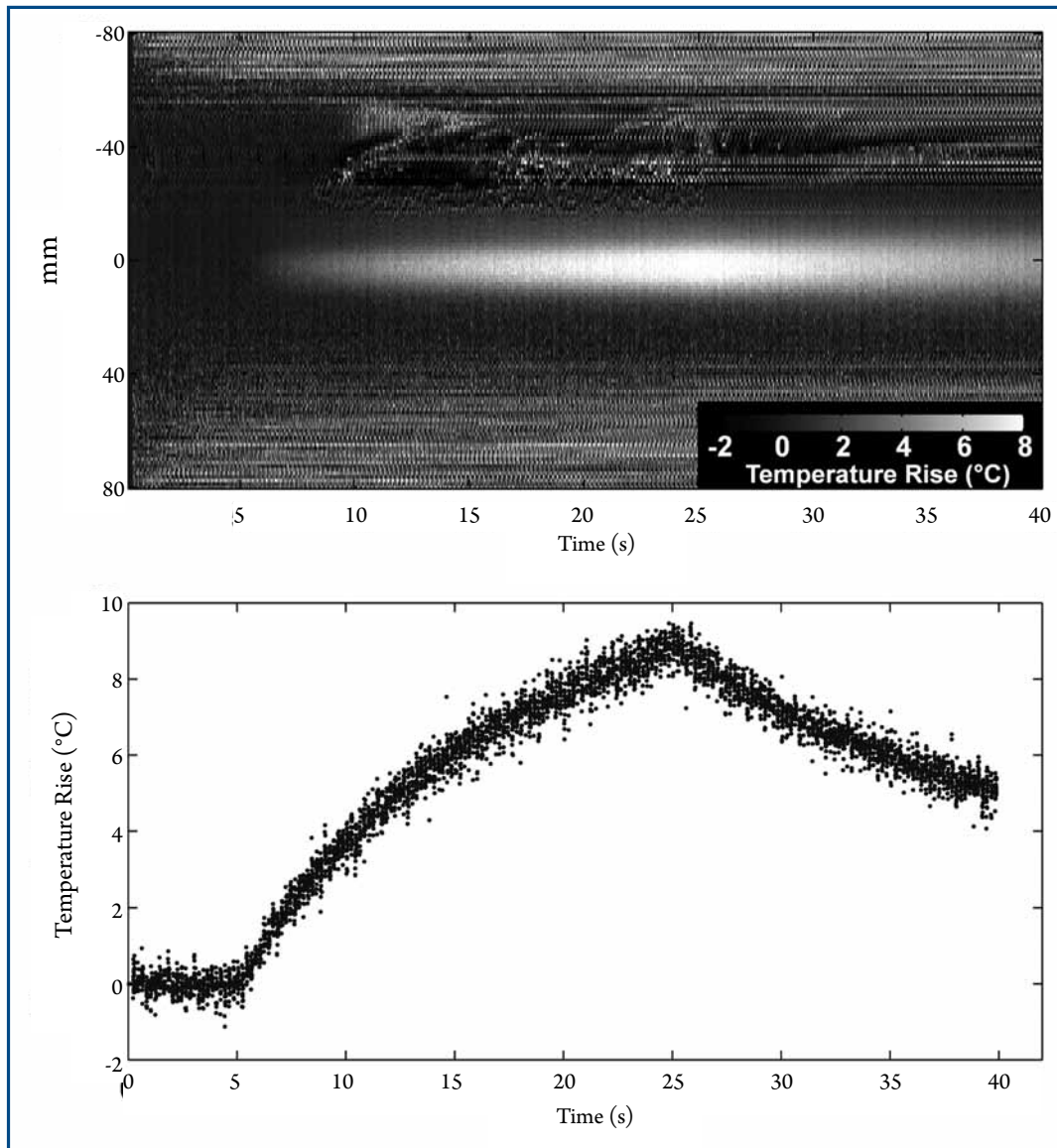


Figure 4. Illustration of 1D temperature measurements during a 20s sonication in a gel phantom using line scan echo-planar spectroscopic imaging at 1.5T. *Up:* This "M-mode" MRI shows the temperature evolution in the line as a function of time. The line was acquired along the direction of the ultrasound beam. By acquiring 32 echoes in one TR of 200 ms and using TE values greater or equal to 27.6 ms, we achieved 4577 measurements in 40 s with a noise level in the imaging with a standard deviation less than $\pm 1^\circ\text{C}$. *Bottom:* Plot of temperature rise vs. time at the focus during the sonication.

compensation methods such as respiration gating, cardiac gating and navigator echoes.

Based on the time scale of the motion with respect to the imaging acquisition time, both intra-scan and inter-scan motion may result during temperature mapping for thermal therapies. Intra-scan motion involves the movement of an object within a single image acquisition time and results in image artifacts

such as ghosts and blurring. Inter-scan motion involves the movement of an object between consecutive image acquisitions and is a problem, especially for temperature mapping in moving organs. Inter-scan motion can result in the misregistration with respect to the baseline phase reference and thus leads to errors in the temperature estimate. The thermal therapy itself can lead to structural change and deformation (usually in the form of



swelling) of the treated tissues due to thermal coagulation.

Respiration represents a major source of motion, especially in the upper abdominal organs, creating significant technical challenges for MR thermometry in the liver. Thermal therapies typically take too long to be performed during a single breath-hold, and require multiple breath-holds or even free-breathing. Normal respiration triggering or gating has been used to effectively compensate the regular and periodical respiration motion (50,51). While respiration gating during free breathing has been demonstrated, it is liable to fail in the presence of irregular breathing patterns (51).

The use of navigator echoes to detect and adapt to the displacement of tissue has been proposed, however, such approaches work best in the presence of rigid body motion, as they do not account for distortion and deformation. A multi-baseline approach combined with respiration triggering and navigator echoes to track diaphragm position has been proposed (52). The method has been applied for temperature mapping of heated *in vivo* porcine kidney and its effectiveness verified in terms of reducing artifacts in temperature maps in the presence of abdominal motion (53).

Alternately, so-called 'referenceless' methods have been proposed to estimate the background (reference) phase from each acquired phase image itself, obviating the need for a baseline reference acquired at a previous time (54). By removing the need for baseline image subtraction, this method supposes to be insensitive to inter-scan motions. In one implementation of this technique, a polynomial is fit to the unwrapped background outside the heating spots using a weighted least-square algorithm. An extrapolation of the fit polynomial into the region where the heating occurs is used as the background phase estimate. This estimate is then subtracted from the acquired phase within the heated regions to obtain the temperature variation map using Eq. 4. Such a referenceless method requires a heating spot that is at least partially surrounded by a nonheated region with sufficiently high signal-to-noise ratio for accurate fitting and reliable extrapolation. Fat suppression is also essential for this technique due to the phase discontinuities between fat and water. This referenceless method has been clinically assessed for temperature mapping of MRI-guided focused ultrasound surgery of uterine fibroids and proved useful for monitoring temperature changes in moving organs (55).

The multibaseline and the referenceless method are compatible and a hybrid approach has been used to combine the strengths of each method and to overcome their individual weakness. The hybrid approach has been shown to be more robust and accurate for temperature mapping of moving organs (56). The proposed multi-pathway sequence mentioned

previously can also be used for both motion tracking of the liver and for temperature mapping (32). Because two pathway images acquired are characterized by different flow properties (the blood vessels in the liver tend to appear dark in the PSIF images and bright in the FISP images), the subtraction of two pathway images yields images of mostly just blood vessels. As such, the liver movement and deformation can be tracked by following the blood vessels inside it (32).

The heart presents an especially difficult challenge for MR thermometry. Preliminary studies (49,57) have shown that high temporal resolution can be reached to resolve the cardiac motion, although further work may be required.

Once tissue motion has been detected and accurate temperature mapping has been achieved, it is necessary to display the dynamic images, temperature-time curves and possibly adjust the thermal treatment procedure in real time based on this information. For example, the focus of the ultrasound array may need to be moved to account for target displacements, or the sonication may need to be stopped if problems are detected or if the therapeutic goals have been reached. Achieving on-line closed loop motion tracking, including feedback and heating control in real-time, may present significant technical challenges. De Senneville *et al.* have recently demonstrated a real-time adaptive method for FUS thermal treatment in mobile organs (58). In their approach, an atlas of motion is constructed with 50 MR images acquired during a pretreatment period without heating. During the thermal therapy, every dynamic image acquired is then compared to the atlas images using an inter-correlation coefficient. The corresponding phase image in the atlas that has the maximum similarity to the dynamic image is used as the reference for temperature mapping. This method assumes periodic and consistent physiological motion but sometimes it may not be well fulfilled even for respiratory motion. The comparison of real-time acquired images with the atlas images imposes an intensive computational burden requiring significant computational capability for high spatial and temporal resolution images. The delay caused by motion pattern calculation, feedback and the execution of focus point adjustment must be small enough to ensure the system can keep up with the motion. A similar idea has also been demonstrated with the combination of a look-up-table-based and a linear-model-based correction for breast thermal treatment that is insensitive to respiratory motion. Other closed-loop, real-time, respiratory-motion-tracking and correction techniques have been also proposed and the reader is referred to the literature for details (53,56,59-63).

The implementation of real-time platforms is essentially crucial for closed loop motion tracking, temperature mapping



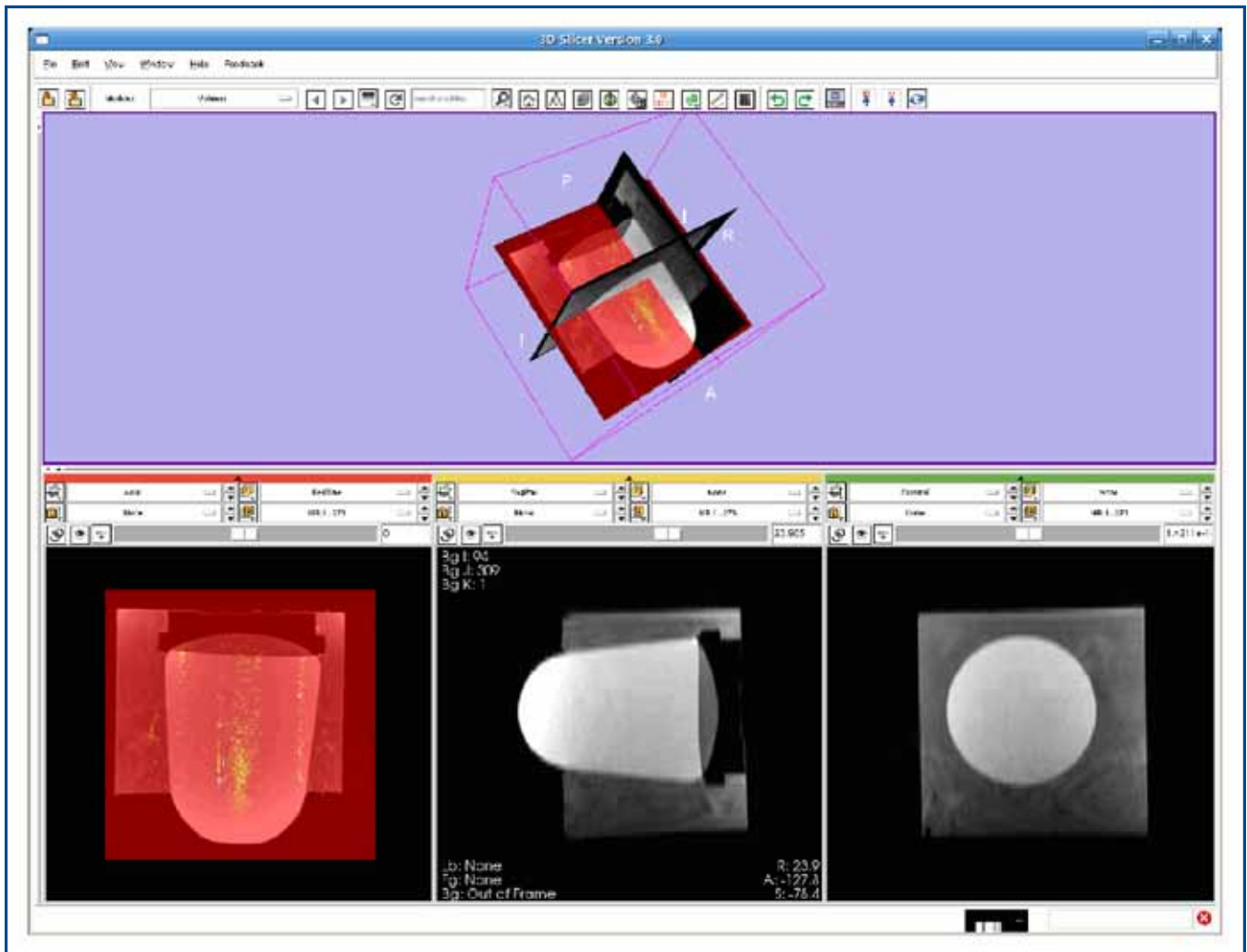


Figure 5. Screenshot of a FUS platform interface for real-time visualization of phantom heating using an open-source software package 3D Slicer. It displays a phantom heating experiment, during which temperature maps were continuously acquired, processed, and displayed. The top panel displays the 3D object and the bottom panel displays three orthogonal tomographic planes of the 3D image. The temperature map is overlaid on the bottom left panel and the heating effect is shown in yellow superimposed on the baseline image. Temperature estimation was updated every 1s with latency of less than 1s.

visualization, and real-time heating control. There are various software packages that could be used as the options for real-time platform for these purposes if motion tracking function and interaction with FUS and MRI scanner are integrated. Figure 5 shows an illustration of a real-time platform for FUS heating experiment on a phantom based on an open-source software package 3D slicer (<http://www.slicer.org/>).

Conclusion

Thermal therapy presents a highly promising opportunity for many clinical applications such as cancer therapy and drug

delivery. MRI is very well suited for guiding such therapies because it is non-invasive, uses non-ionizing-radiation, provides good anatomical images, and proves sensitive to temperature changes. PRF-based temperature imaging has gained special popularity in clinical practice due to the advantages of constant and linear correlation with temperature for aqueous tissues. However, the MR-guidance of thermal therapy in moving organs presents significant challenges that may still preclude widespread use in clinical practice. A number of techniques designed to achieve fast and accurate temperature mapping have been proposed and recent progresses in PRF-based thermometry were reviewed in this article. We believe that, with further development of techniques



such as those discussed here, reliable MR-guidance of thermal therapies in moving organs should prove achievable, and that MR-guided thermal therapy will play an increasingly important role in the treatment of patients worldwide.

Acknowledgments

This work is supported by Hong Kong GRF grant CUHK418811, SEG_CUHK02, and USA NIH grant P41-RR019703.

References

- Lewin JS, Connell CF, Duerk JL, et al. Interactive MRI-guided radiofrequency interstitial thermal ablation of abdominal tumors: clinical trial for evaluation of safety and feasibility. *J Magn Reson Imaging* 1998;8:40-7.
- Sequeiros RB, Hyvönen P, Sequeiros AB, et al. MR imaging-guided laser ablation of osteoid osteomas with use of optical instrument guidance at 0.23 T. *Eur Radiol* 2003;13:2309-14.
- Tempany CM, McDannold NJ, Hynynen K, et al. Focused ultrasound surgery in oncology: overview and principles. *Radiology* 2011;259:39-56.
- Chen J, Daniel BL, Pauly KB. Investigation of proton density for measuring tissue temperature. *J Magn Reson Imaging* 2006;23:430-4.
- Gultekin DH, Gore JC. Temperature dependence of nuclear magnetization and relaxation. *J Magn Reson* 2005;172:133-41.
- Parker DL, Smith V, Sheldon P, et al. Temperature distribution measurements in two-dimensional NMR imaging. *Med Phys* 1983;10:321-5.
- Bottomley PA, Foster TH, Argersinger RE, et al. A review of normal tissue hydrogen NMR relaxation times and relaxation mechanisms from 1-100 MHz: dependence on tissue type, NMR frequency, temperature, species, excision, and age. *Med Phys* 1984;11:425-48.
- Graham SJ, Bronskill MJ, Henkelman RM. Time and temperature dependence of MR parameters during thermal coagulation of ex vivo rabbit muscle. *Magn Reson Med* 1998;39:198-203.
- Le Bihan D, Delannoy J, Levin RL. Temperature mapping with MR imaging of molecular diffusion: application to hyperthermia. *Radiology* 1989;171:853-7.
- Bleier AR, Jolesz FA, Cohen MS, et al. Real-time magnetic resonance imaging of laser heat deposition in tissue. *Magn Reson Med* 1991;21:132-7.
- Young IR, Hand JW, Oatridge A, et al. Modeling and observation of temperature changes in vivo using MRI. *Magn Reson Med* 1994;32:358-69.
- Graham SJ, Stanisz GJ, Kecojec A, et al. Analysis of changes in MR properties of tissues after heat treatment. *Magn Reson Med* 1999;42:1061-71.
- Hindman JC. Proton Resonance Shift of Water in Gas and Liquid States. *Journal of Chemical Physics* 1966;44:4582-8.
- Ishihara Y, Calderon A, Watanabe H, et al. A precise and fast temperature mapping using water proton chemical shift. *Magn Reson Med* 1995;34:814-23.
- De Poorter J. Noninvasive MRI thermometry with the proton resonance frequency method: study of susceptibility effects. *Magn Reson Med* 1995;34:359-67.
- De Poorter J, De Wagter C, De Deene Y, et al. Noninvasive MRI thermometry with the proton resonance frequency (PRF) method: in vivo results in human muscle. *Magn Reson Med* 1995;33:74-81.
- Kuroda K. Non-invasive MR thermography using the water proton chemical shift. *Int J Hyperthermia* 2005;21:547-60.
- Kuroda K, Takei N, Mulkern RV, et al. Feasibility of internally referenced brain temperature imaging with a metabolite signal. *Magn Reson Med Sci* 2003;2:17-22.
- Kuroda K, Mulkern RV, Oshio K, et al. Temperature mapping using the water proton chemical shift: self-referenced method with echo-planar spectroscopic imaging. *Magn Reson Med* 2000;43:220-5.
- McDannold N, Hynynen K, Oshio K, et al. Temperature monitoring with line scan echo planar spectroscopic imaging. *Med Phys* 2001;28:346-55.
- McDannold N. Quantitative MRI-based temperature mapping based on the proton resonant frequency shift: review of validation studies. *Int J Hyperthermia* 2005;21:533-46.
- Hore PJ. Nuclear magnetic resonance. Oxford: Oxford University Press;1995:90.
- Kuroda K, Oshio K, Mulkern RV, et al. Optimization of chemical shift selective suppression of fat. *Magn Reson Med* 1998;40:505-10.
- Vogel MW, Pattynama PM, Lethimonnier FL, et al. Use of fast spin echo for phase shift magnetic resonance thermometry. *J Magn Reson Imaging* 2003;18:507-12.
- Cline HE, Hynynen K, Schneider E, et al. Simultaneous magnetic resonance phase and magnitude temperature maps in muscle. *Magn Reson Med* 1996;35:309-15.
- de Zwart JA, Vimeux FC, Delalande C, et al. Fast lipid-suppressed MR temperature mapping with echo-shifted gradient-echo imaging and spectral-spatial excitation. *Magn Reson Med* 1999;42:53-9.
- Weidensteiner C, Quesson B, Caire-Gana B, et al. Real-time MR temperature mapping of rabbit liver in vivo during thermal ablation. *Magn Reson Med* 2003;50:322-30.
- Stafford RJ, Price RE, Diederich CJ, et al. Interleaved echo-planar imaging for fast multiplanar magnetic resonance temperature imaging of ultrasound thermal ablation therapy. *J Magn Reson Imaging* 2004;20:706-14.
- Stafford RJ, Hazle JD, Glover GH. Monitoring of high-intensity focused ultrasound-induced temperature changes in vitro using an interleaved spiral acquisition. *Magn Reson Med* 2000;43:909-12.
- Scheffler K. Fast frequency mapping with balanced SSFP: theory and application to proton-resonance frequency shift thermometry. *Magn Reson Med* 2004;51:1205-11.
- Paliwal V, El-Sharkawy AM, Du X, et al. SSFP-based MR thermometry. *Magn Reson Med* 2004;52:704-8.
- Madore B, Panych LP, Mei CS, et al. Multipathway sequences for MR thermometry. *Magn Reson Med* 2011;66:658-68.
- Kuroda K, Oshio K, Chung AH, et al. Temperature mapping using the



- water proton chemical shift: a chemical shift selective phase mapping method. *Magn Reson Med* 1997;38:845-51.
34. Yuan J, Mei CS, Madore B, et al. Fast fat-suppressed reduced field-of-view temperature mapping using 2DRF excitation pulses. *J Magn Reson* 2011;210:38-43.
 35. Fleckenstein JL, Archer BT, Barker BA, et al. Fast short-tau inversion-recovery MR imaging. *Radiology* 1991;179:499-504.
 36. Meyer CH, Pauly JM, Macovski A, et al. Simultaneous spatial and spectral selective excitation. *Magn Reson Med* 1990;15:287-304.
 37. Yuan J, Madore B, Panych LP. Fat-water selective excitation in balanced steady-state free precession using short spatial-spectral RF pulses. *J Magn Reson* 2011;208:219-24.
 38. Rieke V, Butts Pauly K. Echo combination to reduce proton resonance frequency (PRF) thermometry errors from fat. *J Magn Reson Imaging* 2008;27:673-7.
 39. Glover GH, Schneider E. Three-point Dixon technique for true water/fat decomposition with B0 inhomogeneity correction. *Magn Reson Med* 1991;18:371-83.
 40. Glover GH. Multipoint Dixon technique for water and fat proton and susceptibility imaging. *J Magn Reson Imaging* 1991;1:521-30.
 41. Dixon WT. Simple proton spectroscopic imaging. *Radiology* 1984;153(1):189-94.
 42. Reeder SB, Wen Z, Yu H, et al. Multicoil Dixon chemical species separation with an iterative least-squares estimation method. *Magn Reson Med* 2004;51:35-45.
 43. Soher BJ, Wyatt C, Reeder SB, et al. Noninvasive temperature mapping with MRI using chemical shift water-fat separation. *Magn Reson Med* 2010;63:1238-46.
 44. Zhao L, Madore B, Panych LP. Reduced field-of-view MRI with two-dimensional spatially-selective RF excitation and UNFOLD. *Magn Reson Med* 2005;53:1118-25.
 45. Mei CS, Panych LP, Yuan J, et al. Combining two-dimensional spatially selective RF excitation, parallel imaging, and UNFOLD for accelerated MR thermometry imaging. *Magn Reson Med* 2011;66:112-22.
 46. Madore B, Glover GH, Pelc NJ. Unaliasing by fourier-encoding the overlaps using the temporal dimension (UNFOLD), applied to cardiac imaging and fMRI. *Magn Reson Med* 1999;42:813-28.
 47. Panych LP, Zhao L, Jolesz FA, et al. Dynamic imaging with multiple resolutions along phase-encode and slice-select dimensions. *Magn Reson Med* 2001;45:940-7.
 48. Aljallad MH, Yuan J, Pilatou MC, et al. Multiresolution MRI temperature monitoring in a reduced field of view. *Magn Reson Imaging* 2011;29:1205-14.
 49. Mei CS, Mulkern RV, Oshio K, et al. Ultrafast 1D MR thermometry using phase or frequency mapping. *MAGMA* 2011. [Epub ahead of print]
 50. Morikawa S, Inubushi T, Kurumi Y, et al. Feasibility of respiratory triggering for MR-guided microwave ablation of liver tumors under general anesthesia. *Cardiovasc Intervent Radiol* 2004;27:370-3.
 51. Lepetit-Coiffé M, Quesson B, Seror O, et al. Real-time monitoring of radiofrequency ablation of rabbit liver by respiratory-gated quantitative temperature MRI. *J Magn Reson Imaging* 2006;24:152-9.
 52. Vigen KK, Daniel BL, Pauly JM, et al. Triggered, navigated, multi-baseline method for proton resonance frequency temperature mapping with respiratory motion. *Magn Reson Med* 2003;50:1003-10.
 53. Köhler MO, Denis de Senneville B, Quesson B, et al. Spectrally selective pencil-beam navigator for motion compensation of MR-guided high-intensity focused ultrasound therapy of abdominal organs. *Magn Reson Med* 2011;66:102-11.
 54. Rieke V, Vigen KK, Sommer G, et al. Referenceless PRF shift thermometry. *Magn Reson Med* 2004;51:1223-31.
 55. McDannold N, Tempny C, Jolesz F, et al. Evaluation of referenceless thermometry in MRI-guided focused ultrasound surgery of uterine fibroids. *J Magn Reson Imaging* 2008;28:1026-32.
 56. Grissom WA, Rieke V, Holbrook AB, et al. Hybrid referenceless and multibaseline subtraction MR thermometry for monitoring thermal therapies in moving organs. *Med Phys* 2010;37:5014-26.
 57. Hey S, Cernicanu A, de Senneville BD, et al. Towards optimized MR thermometry of the human heart at 3T. *NMR Biomed* 2012;25:35-43.
 58. de Senneville BD, Mougnot C, Moonen CT. Real-time adaptive methods for treatment of mobile organs by MRI-controlled high-intensity focused ultrasound. *Magn Reson Med* 2007;57:319-30.
 59. Maier F, Krafft AJ, Yung JP, et al. Velocity navigator for motion compensated thermometry. *MAGMA* 2011. [Epub ahead of print]
 60. Wyatt CR, Soher BJ, MacFall JR. Correction of breathing-induced errors in magnetic resonance thermometry of hyperthermia using multiecho field fitting techniques. *Med Phys* 2010;37:6300-9.
 61. Todd N, Payne A, Parker DL. Model predictive filtering for improved temporal resolution in MRI temperature imaging. *Magn Reson Med* 2010;63:1269-79.
 62. Roujol S, Ries M, Quesson B, et al. Real-time MR-thermometry and dosimetry for interventional guidance on abdominal organs. *Magn Reson Med* 2010;63:1080-7.
 63. Ries M, de Senneville BD, Roujol S, Berber Y, et al. Real-time 3D target tracking in MRI guided focused ultrasound ablations in moving tissues. *Magn Reson Med* 2010;64:1704-12.

Cite this article as: Yuan J, Mei CS, Panych LP, McDannold NJ, Madore B. Towards fast and accurate temperature mapping with proton resonance frequency-based MR thermometry. *Quant Imaging Med Surg* 2012;2:21-32. DOI: 10.3978/j.issn.2223-4292.2012.01.06

